ESAIM: M2AN 50 (2016) 1269–1287
DOI: 10.1051/m2an/2015078

ESAIM: Mathematical Modelling and Numerical Analysis
www.esaim-m2an.org

QUALITATIVE BEHAVIOUR AND NUMERICAL APPROXIMATION OF SOLUTIONS TO CONSERVATION LAWS WITH NON-LOCAL POINT CONSTRAINTS ON THE FLUX AND MODELING OF CROWD DYNAMICS AT THE BOTTLENECKS

Boris Andreianov[1,2], Carlotta Donadello[1],
Ulrich Razafison[1] and Massimiliano D. Rosini[3]

Abstract. In this paper we investigate numerically the model for pedestrian traffic proposed in [B. Andreianov, C. Donadello, M.D. Rosini, *Math. Models Methods Appl. Sci.* **24** (2014) 2685−2722]. We prove the convergence of a scheme based on a constraint finite volume method and validate it with an explicit solution obtained in the above reference. We then perform *ad hoc* simulations to qualitatively validate the model under consideration by proving its ability to reproduce typical phenomena at the bottlenecks, such as Faster Is Slower effect and the Braess' paradox.

Mathematics Subject Classification. 35L65, 90B20, 65M12, 76M12.

Received March 31, 2015. Revised October 4, 2015. Accepted October 11, 2015.

1. Introduction

Andreianov, Donadello and Rosini developed in [5] a macroscopic model, called here ADR, aiming at describing the behaviour of pedestrians at bottlenecks. The model is given by the Cauchy problem for a scalar hyperbolic conservation law in one space dimension with non-local point constraint of the form

$$\partial_t \rho + \partial_x f(\rho) = 0 \qquad (t,x) \in \mathbb{R}_+ \times \mathbb{R}, \tag{1.1a}$$

$$\rho(0,x) = \bar{\rho}(x) \qquad x \in \mathbb{R}, \tag{1.1b}$$

$$f\left(\rho(t,0\pm)\right) \leq p\left(\int_{\mathbb{R}_-} w(x)\ \rho(t,x)\ \mathrm{d}x\right) \qquad t \in \mathbb{R}_+, \tag{1.1c}$$

Keywords and phrases. Finite volume scheme, scalar conservation law, non-local point constraint, crowd dynamics, capacity drop, Braess' paradox, Faster Is Slower.

[1] Laboratoire de Mathématiques de Besançon, UMR CNRS 6623, Université de Franche-Comté, 25030 16 route de Gray, 25030 Besançon cedex, France. boris.andreianov@univ-fcomte.fr; carlotta.donadello@univ-fcomte.fr; ulrich.razafison@univ-fcomte.fr

[2] LMPT CNRS UMR 7350, 37200 Tours, France. boris.andreianov@lmpt.univ-tours.fr

[3] Instytut Matematyki, Uniwersytet Marii Curie-Skłodowskiej, pl. Marii Curie-Skłodowskiej 5, 20-031 Lublin, Poland. mrosini@hektor.umcs.lublin.pl

Article published by EDP Sciences

where $\rho(t,x) \in [0,R]$ is the (mean) density of pedestrians at $x \in \mathbb{R}$ at time $t \in \mathbb{R}_+$ and $\bar\rho\colon \mathbb{R} \to [0,R]$ is the initial (mean) density, with $R>0$ being the maximal density. Then, $f\colon [0,R] \to \mathbb{R}_+$ is the flow considered to be bell-shaped, which is an assumption commonly used in crowd dynamics (see [13,15,32] for examples of non bell-shaped flows used in crowd dynamics and [2,11,12] for the numerical approximations). A typical example of such flow is the so-called Lighthill–Whitham–Richards (LWR) flux [20,29,31] defined by

$$f(\rho) = \rho\, v_{\max}\left(1 - \frac{\rho}{\rho_{\max}}\right),$$

where $v_{\max}$ and $\rho_{\max}$ are the maximal velocity and the maximal density of pedestrians respectively. Throughout this paper the LWR flux will be used. Next, $p\colon \mathbb{R}_+ \to \mathbb{R}_+$ prescribes the maximal flow allowed through a bottleneck located at $x=0$ as a function of the weighted average density in a left neighbourhood of the bottleneck and $w\colon \mathbb{R}_- \to \mathbb{R}_+$ is the weight function used to average the density.

Finally in (1.1c), $\rho(t,0-)$ denotes the left measure theoretic trace along the constraint, implicitly defined by

$$\lim_{\varepsilon\downarrow 0}\frac{1}{\varepsilon}\int_0^{+\infty}\int_{-\varepsilon}^{0} |\rho(t,x)-\rho(t,0-)|\;\phi(t,x)\;\mathrm{d}x\;\mathrm{d}t = 0 \qquad \text{for all } \phi \in \mathbf{C}_{\mathbf{c}}^{\infty}(\mathbb{R}^2;\mathbb{R}).$$

The right measure theoretic trace, $\rho(t,0+)$, is defined analogously.

In the last few decades, the study of the pedestrian behaviour through bottlenecks, namely at locations with reduced capacity, such as doors, stairs or narrowings, drawn a considerable attention. The papers [9,23,25,26,34,35,38] present results of empirical experiments. However, for safety reasons, experiments reproducing extremal conditions such as evacuation and stampede are not available. In fact, the unique experimental study of a crowd disaster is proposed in [22]. The available data show that the capacity of the bottleneck (*i.e.* the maximum number of pedestrians that can flow through the bottleneck in a given time interval) can drop when high-density conditions occur upstream of the bottleneck. This phenomenon is called *capacity drop* and can lead to extremely serious consequences in escape situations. In fact, the crowd pressure before an exit can reach very high values, the efficiency of the exit dramatically reduces and accidents become more probable due to the overcrowding and the increase of the evacuation time (*i.e.* the temporal gap between the times in which the first and the last pedestrian pass through the bottleneck). A linked phenomenon is the so-called *Faster Is Slower* (FIS) effect, first described in [21]. FIS effect refers to the jamming and clogging at the bottlenecks, that result in an increase of the evacuation time when the degree of hurry of a crowd is high. We recall that the capacity drop and the FIS effect are both experimentally reproduced in [9,36]. A further related (partly counter-intuitive) phenomenon is the so-called *Braess' paradox* for pedestrian flows [24]. It is well known that placing a small obstacle before an exit door can mitigate the inter-pedestrian pressure and, under particular circumstances, it reduces the evacuation time by improving the outflow of people.

Note that as it happens for any first order model, see for instance ([33], Part III) and the references therein, ADR can not explain the capacity drop and collective behaviours at the bottlenecks. Therefore one of the difficulties we have to face is that the constraint p has to be deduced together with the fundamental diagram from the empirical observations.

The aim of this paper is to validate ADR by performing simulations in order to show the ability of the model to reproduce the main effects described above and related to capacity drop that are FIS and Braess' paradox. To this end we propose a numerical scheme for the model and prove its convergence. The scheme is obtained by adapting the local constrained finite volume method introduced in [3] to the non-local case considered in ADR, using a splitting strategy.

The paper is organized as follows. In Section 2 we briefly recall the main theoretical results for ADR. In Section 3 we introduce the numerical scheme, prove its convergence and validate it with an explicit solution obtained in [5]. In Section 4 we perform simulations to show that ADR is able to reproduce the Braess' paradox and the FIS effect. In Section 4.3 we combine local and non-local constraints to model a slow zone placed before the exit. Conclusions and perspectives are outlined in Section 5.

2. Well-posedness for the ADR model

Existence, uniqueness and stability for the general Cauchy problem (1.1) are established in [5] under the following assumptions:

(F) f belongs to $\mathbf{Lip}([0,R];[0,+\infty[)$ and is supposed to be bell-shaped, that is $f(0)=0=f(R)$ and there exists $\sigma\in\,]0,R[$ such that $f'(\rho)\,(\sigma-\rho)>0$ for a.e. $\rho\in[0,R]$.

(W) w belongs to $\mathbf{L}^\infty(\mathbb{R}_-;\mathbb{R}_+)$, is an increasing map, $\|w\|_{\mathbf{L}^1(\mathbb{R}_-)}=1$ and there exists $\mathrm{i}_w>0$ such that $w(x)=0$ for any $x\le-\mathrm{i}_w$.

(P) p belongs to $\mathbf{Lip}([0,R]\,;]0,f(\sigma)])$ and is a non-increasing map.

The regularity $w\in\mathbf{L}^\infty(\mathbb{R}_-;\mathbb{R}_+)$ is the minimal requirement needed in order to prove existence and uniqueness of (1.1). In this paper, we shall consider continuous w.

The existence of solutions for the Riemann problem for (1.1) is proved in [6] for piecewise constant p. However, such hypothesis on p is not sufficient to ensure uniqueness of solutions, unless the flux f and the efficiency p satisfy a simple geometric condition, see [6] for details. In the present paper, we consider either continuous nonlinear p or a piecewise constant p that satisfies such geometric condition.

The definition of entropy solution for a Cauchy problem (1.1a), (1.1b) with a fixed *a priori* time dependent constraint condition

$$f\left(\rho(t,0\pm)\right)\le q(t)\qquad\qquad t\in\mathbb{R}_+ \tag{2.1}$$

was introduced in ([14], Def. 3.2) and then reformulated in ([3], Def. 2.1), see also ([3], Prop. 2.6 and [12], Def. 2.2). Such definitions are obtained by adding a term that accounts for the constraint in the classical definition of entropy solution given by Kruzhkov in ([27], Def. 1). The definition of entropy solution given in ([5], Def. 2.1) is obtained by extending these definitions to the framework of non-local constraints. It worths noticing that the theory of conservation laws subject to point constraints as initiated in [14] is related to the theory of conservation laws with discontinuous flux functions. Indeed a limitation of the flux of the form (2.1) can be interpreted as the choice of an (A,B)-connection if the problem is reformulated as a discontinuous flux problem, see [4] for a full theoretical discussion of this point and [1,2,10] for related numerical investigations.

The following theorem on existence, uniqueness and stability of entropy solutions of the constrained Cauchy problem (1.1) is achieved under the hypotheses **(F)**, **(W)** and **(P)**.

Theorem 2.1 (Thm. 3.1 in [5])**.** *Let* **(F)**, **(W)**, **(P)** *hold. Then, for any initial datum* $\bar\rho\in\mathbf{L}^\infty(\mathbb{R};[0,R])$*, the Cauchy problem* (1.1) *admits a unique entropy solution* ρ*. Moreover, if* $\rho'=\rho'(t,x)$ *is the entropy solution corresponding to the initial datum* $\bar\rho'\in\mathbf{L}^\infty(\mathbb{R};[0,R])$*, then for all* $T>0$ *and* $L>\mathrm{i_w}$*, the following inequality holds*

$$\|\rho(T)-\rho'(T)\|_{\mathbf{L}^1([-L,L])}\le e^{CT}\|\bar\rho-\bar\rho'\|_{\mathbf{L}^1(\{|x|\le L+MT\})}, \tag{2.2}$$

where $M=\mathrm{Lip}(f)$ *and* $C=2\mathrm{Lip}(p)\|w\|_{\mathbf{L}^\infty(\mathbb{R}_-)}$.

The total variation of the solution may in general increase due to the presence of the constraint. In [5] the authors provide an invariant domain $\mathcal{D}\subset\mathbf{L}^1(\mathbb{R};[0,R])$ such that if $\bar\rho$ belongs to $\mathcal{D}$, then one obtains a Lipschitz estimate with respect to time of the $\mathbf{L}^1$ norm and an *a priori* estimate of the total variation of

$$\Psi(\rho)=\mathrm{sign}(\rho-\sigma)[f(\sigma)-f(\rho)]=\int_\sigma^\rho\left|\dot f(r)\right|\mathrm{d}r.$$

3. Numerical method for approximation of ADR

In this section we describe the numerical scheme based on finite volume method that we use to solve (1.1). Then we prove the convergence of our scheme and validate it by comparison with an explicit solution of (1.1). In what follows, we assume that **(F)**, **(W)** and **(P)** hold.

3.1. Non-local constrained finite volume method

Let Δx and Δt be the constant space and time steps respectively. We define the points $x_{j+1/2} = j\Delta x$, the cells $K_j = [x_{j-1/2}, x_{j+1/2}[$ and the cell centers $x_j = (j-1/2)\Delta x$ for $j \in \mathbb{Z}$. We define the time discretization $t^n = n\Delta t$. We introduce the index j_c such that $x_{j_c+1/2}$ is the location of the constraint (a door or an obstacle). For $n \in \mathbb{N}$ and $j \in \mathbb{Z}$, we denote by ρ_j^n the approximation of the average of $\rho(t^n, \cdot\,)$ on the cell K_j, namely

$$\rho_j^0 = \frac{1}{\Delta x}\int_{x_{j-1/2}}^{x_{j+1/2}} \overline{\rho}(x)\,\mathrm{d}x \qquad \text{and} \qquad \rho_j^n \simeq \frac{1}{\Delta x}\int_{x_{j-1/2}}^{x_{j+1/2}} \rho(t^n, x)\,\mathrm{d}x \qquad \text{if } n > 0.$$

We recall that for the classical conservation law (1.1a)–(1.1b), a standard finite volume method can be written into the form

$$\rho_j^{n+1} = \rho_j^n - \frac{\Delta t}{\Delta x}\left(\mathcal{F}_{j+1/2}^n - \mathcal{F}_{j-1/2}^n\right), \tag{3.1}$$

where $\mathcal{F}_{j+1/2}^n = F\left(\rho_j^n, \rho_{j+1}^n\right)$ is a monotone, consistent numerical flux, that is, F satisfies the following assumptions:

- F is Lipschitz continuous from $[0,R]^2$ to $\mathbb{R}$ with Lipschitz constant $\mathrm{Lip}(F)$,
- $F(a,a) = f(a)$ for any $a \in [0,R]$,
- $(a,b) \in [0,R]^2 \mapsto F(a,b) \in \mathbb{R}$ is non-decreasing with respect to a and non-increasing with respect to b.

We also recall that in [3] the numerical flux for the time dependent constraint (2.1) is modified as follow in order to take into account the constraint condition

$$\mathcal{F}_{j+1/2}^n = \begin{cases} F\left(\rho_j^n, \rho_{j+1}^n\right) & \text{if } j \neq j_c, \\ \min\left\{F\left(\rho_j^n, \rho_{j+1}^n\right), q^n\right\} & \text{if } j = j_c, \end{cases} \tag{3.2}$$

where q^n is an approximation of $q(t^n)$. In the present paper, when dealing with a Cauchy problem subject to a non-local constraint of the form (1.1c) we will use the approximation

$$q^n = p\left(\Delta x \sum_{j \le j_c} w(x_j)\,\rho_j^n\right). \tag{3.3}$$

Roughly speaking

- we apply the numerical scheme (3.1) for the problem (1.1a) and (1.1b),
- we apply the numerical scheme (3.1)–(3.2) for the problem (1.1a), (1.1b) and (2.1),
- we apply the numerical scheme (3.1)–(3.3) for the problem (1.1).

3.2. Convergence of the scheme

Let us introduce the finite volume approximate solution ρ_Δ defined by

$$\rho_\Delta(t,x) = \rho_j^n \qquad \text{for } x \in K_j \text{ and } t \in [t^n, t^{n+1}[, \tag{3.4}$$

where the sequence $(\rho_j^n)_{j\in\mathbb{Z},\, n\in\mathbb{N}}$ is obtained by the numerical scheme (3.1) and (3.2). Analogously, we also define the approximate constraint function

$$q_\Delta(t) = q^n \qquad \text{for } t \in [t^n, t^{n+1}[. \tag{3.5}$$

First, we prove a discrete stability estimate valid for any domain $Q = [0,T] \times \mathbb{R}$ with $T > 0$, for the scheme (3.1)–(3.2) applied to problem (1.1a), (1.1b) and (2.1). This estimate can be seen as the equivalent, in this framework, of the stability result established in ([3], Prop. 2.10).

Proposition 3.1. *Let $\overline{\rho}$ be in $\mathbf{L}^\infty(\mathbb{R};[0,R])$ and q_Δ, $\hat{q}_\Delta$ be piecewise constant functions of the form (3.5). If ρ_Δ and $\hat{\rho}_\Delta$ are the approximate solutions of (1.1a), (1.1b) and (2.1) corresponding, respectively, to q_Δ and $\hat{q}_\Delta$ and constructed by applying the scheme (3.1)–(3.2), then we have*

$$\|\rho_\Delta - \hat{\rho}_\Delta\|_{\mathbf{L^1}(Q)} \leq 2T\|q_\Delta - \hat{q}_\Delta\|_{\mathbf{L^1}([0,T])}.$$

Proof. For notational simplicity, let $N = \lfloor T/\Delta t \rfloor$. Let us also introduce $(\tilde{\rho}_j^n)_{j\in\mathbb{Z},\, n\in\mathbb{N}}$ defined by,

$$\tilde{\rho}_j^{n+1} = \rho_j^n - \frac{\Delta t}{\Delta x}\left(\tilde{\mathcal{F}}_{j+1/2}^n - \tilde{\mathcal{F}}_{j-1/2}^n\right), \quad \text{for any } j\in\mathbb{Z},\, n\in\mathbb{N},$$

where $\tilde{\mathcal{F}}_{j+1/2}^n$ is defined by

$$\tilde{\mathcal{F}}_{j+1/2}^n = \begin{cases} F\left(\rho_j^n, \rho_{j+1}^n\right) & \text{if } j \neq j_c, \\ \min\left\{F\left(\rho_j^n, \rho_{j+1}^n\right), \hat{q}^n\right\} & \text{if } j = j_c. \end{cases}$$

Then using the definitions of $(\rho_j^n)_{j\in\mathbb{Z},\, n\in\mathbb{N}}$ and $(\tilde{\rho}_j^n)_{j\in\mathbb{Z},\, n\in\mathbb{N}}$, we have for any $n = 1,\dots,N$,

$$\rho_j^n = \tilde{\rho}_j^n \quad \text{if} \quad j \notin \{j_c, j_c+1\}$$

and

$$\rho_{j_c}^n - \tilde{\rho}_{j_c}^n = -\frac{\Delta t}{\Delta x}\left(\min\left\{F\left(\rho_{j_c}^{n-1}, \rho_{j_c+1}^{n-1}\right), q^{n-1}\right\} - \min\left\{F\left(\rho_{j_c}^{n-1}, \rho_{j_c+1}^{n-1}\right), \hat{q}^{n-1}\right\}\right),$$
$$\rho_{j_c+1}^n - \tilde{\rho}_{j_c+1}^n = \frac{\Delta t}{\Delta x}\left(\min\left\{F\left(\rho_{j_c}^{n-1}, \rho_{j_c+1}^{n-1}\right), q^{n-1}\right\} - \min\left\{F\left(\rho_{j_c}^{n-1}, \rho_{j_c+1}^{n-1}\right), \hat{q}^{n-1}\right\}\right),$$

which implies that

$$\left|\rho_{j_c}^n - \tilde{\rho}_{j_c}^n\right| \leq \frac{\Delta t}{\Delta x}\left|q^{n-1} - \hat{q}^{n-1}\right|, \qquad \left|\rho_{j_c+1}^n - \tilde{\rho}_{j_c+1}^n\right| \leq \frac{\Delta t}{\Delta x}\left|q^{n-1} - \hat{q}^{n-1}\right|.$$

Therefore we deduce that, for any $n = 1,\dots,N$,

$$\sum_{j\in\mathbb{Z}}\left|\rho_j^n - \tilde{\rho}_j^n\right| \leq 2\frac{\Delta t}{\Delta x}\left|q^{n-1} - \hat{q}^{n-1}\right|. \tag{3.6}$$

Besides, observe that the modification of the numerical flux at the interface $x_{j_c+1/2}$ introduced in (3.2) does not affect the monotonicity of the scheme (3.1)–(3.2) (see [3], Prop. 4.2). Therefore, for any $n = 1,\dots,N$, we have

$$\sum_{j\in\mathbb{Z}}\left|\tilde{\rho}_j^n - \hat{\rho}_j^n\right| \leq \sum_{j\in\mathbb{Z}}\left|\rho_j^{n-1} - \hat{\rho}_j^{n-1}\right|. \tag{3.7}$$

Hence thanks to (3.6) and (3.7), we can write

$$\sum_{j\in\mathbb{Z}}|\rho_j^1 - \hat{\rho}_j^1| \leq \sum_{j\in\mathbb{Z}}|\rho_j^1 - \tilde{\rho}_j^1| + \sum_{j\in\mathbb{Z}}|\tilde{\rho}_j^1 - \hat{\rho}_j^1| \leq 2\frac{\Delta t}{\Delta x}\left|q^0 - \hat{q}^0\right| + \sum_{j\in\mathbb{Z}}|\rho_j^0 - \hat{\rho}_j^0| = 2\frac{\Delta t}{\Delta x}\left|q^0 - \hat{q}^0\right|.$$

Then an induction argument shows that for any $n = 1,\dots,N$,

$$\sum_{j\in\mathbb{Z}}\left|\rho_j^n - \hat{\rho}_j^n\right| \leq 2\frac{\Delta t}{\Delta x}\sum_{k=0}^{n-1}|q^k - \hat{q}^k| \leq \frac{2}{\Delta x}\,\|q_\Delta - \hat{q}_\Delta\|_{L^1([0,t^n])}.$$

In conclusion, we find that

$$\|\rho_\Delta - \hat{\rho}_\Delta\|_{L^1(Q)} = \Delta t\,\Delta x\sum_{n=1}^{N}\sum_{j\in\mathbb{Z}}|\rho_j^n - \hat{\rho}_j^n| \leq 2\|q_\Delta - \hat{q}_\Delta\|_{L^1([0,T])}\sum_{n=1}^{N}\Delta t \leq 2T\|q_\Delta - \hat{q}_\Delta\|_{L^1([0,T])}$$

and this ends the proof. □

Let us now notice that as in ([3], Prop. 4.2), under the CFL condition

$$\mathrm{Lip}(F)\ \frac{\Delta t}{\Delta x} \le \frac{1}{2}, \tag{3.8}$$

we have the $\mathbf{L}^\infty$ stability of the scheme (3.1)-(3.2)-(3.3) that is

$$0 \le \rho_\Delta(t,x) \le R \qquad \text{for a.e. } (t,x) \in Q. \tag{3.9}$$

This stability result allows to prove the statement below.

Proposition 3.2. *Let q_Δ be defined by (3.3)−(3.5). Assume moreover that w belongs to $\mathbf{Lip}(\mathbb{R}_-;\mathbb{R}_+)$. Then under the CFL condition (3.8), for any $T>0$, there exists $C>0$ only depending on T, f, F, p, w and R such that:*

$$|q_\Delta|_{BV([0,T])} \le C. \tag{3.10}$$

Proof. Let $N=\lfloor T/\Delta t\rfloor$ and j_w be an integer such that $\mathrm{supp}(w) \subset \underset{j_w\le j\le j_c}{\cup} K_j$. Then for any $n=0,\dots,N-1$, we have

$$\begin{aligned}\left|q^{n+1}-q^n\right| &= \left|p\left(\Delta x \sum_{j_w\le j\le j_c} w(x_j)\rho_j^{n+1}\right) - p\left(\Delta x \sum_{j_w\le j\le j_c} w(x_j)\rho_j^{n}\right)\right| \\ &\le \Delta x\,\mathrm{Lip}(p)\left|\sum_{j_w\le j\le j_c} w(x_j)(\rho_j^{n+1}-\rho_j^n)\right| = \Delta t\,\mathrm{Lip}(p)\left|\sum_{j_w\le j\le j_c} w(x_j)\left(\mathcal{F}_{j+1/2}^n-\mathcal{F}_{j-1/2}^n\right)\right|.\end{aligned}$$

Now, using a summation by part, we have

$$\sum_{j_w\le j\le j_c} w(x_j)\left(\mathcal{F}_{j+1/2}^n-\mathcal{F}_{j-1/2}^n\right) = w(x_{j_c})\mathcal{F}_{j_c+1/2}^n - w(x_{j_w})\mathcal{F}_{j_w-1/2}^n - \sum_{j_w\le j\le j_c-1}\left(w(x_{j+1})-w(x_j)\right)\mathcal{F}_{j+1/2}^n.$$

Then, using the fact that w belongs to $\mathbf{Lip}(\mathbb{R}_-;\mathbb{R}_+)$, it follows that

$$\sum_{j_w\le j\le j_c} w(x_j)\left(\mathcal{F}_{j+1/2}^n-\mathcal{F}_{j-1/2}^n\right) \le \|w\|_{\mathbf{L}^\infty(\mathbb{R}_-;\mathbb{R}_+)}\left(|\mathcal{F}_{j_c+1/2}^n| + |\mathcal{F}_{j_w-1/2}^n|\right) + \Delta x\,\mathrm{Lip}(w)\sum_{j_w\le j\le j_c-1}|\mathcal{F}_{j+1/2}^n|.$$

This yields

$$|q^{n+1}-q^n| \le \Delta t\,\mathrm{Lip}(p)\|w\|_{\mathbf{L}^\infty(\mathbb{R}_-;\mathbb{R})}\left(|\mathcal{F}_{j_c+1/2}^n| + |\mathcal{F}_{j_w-1/2}^n|\right) + \Delta t\Delta x\,\mathrm{Lip}(p)\,\mathrm{Lip}(w)\sum_{j_w\le j\le j_c-1}|\mathcal{F}_{j+1/2}^n|.$$

Now, from (3.2), for any $j\in\mathbb{Z}$ we have the estimate

$$\begin{aligned}\left|\mathcal{F}_{j+1/2}^n\right| &\le \left|F(\rho_j^n,\rho_{j+1}^n)\right| \le \left|F(\rho_j^n,\rho_{j+1}^n)-F(\rho_j^n,\rho_j^n)\right| + \left|f(\rho_j^n)\right| \\ &\le \mathrm{Lip}(F)\left|\rho_{j+1}^n-\rho_j^n\right| + \mathrm{Lip}(f)\left|\rho_j^n\right| \le R\left(\mathrm{Lip}(F)+\mathrm{Lip}(f)\right).\end{aligned}$$

Hence we deduce that

$$|q_\Delta|_{BV([0,T])} = \sum_{n=0}^{N-1}|q^{n+1}-q^n| \le C,$$

where $C = T\,\mathrm{Lip}(p)\left(R(\mathrm{Lip}(F)+\mathrm{Lip}(f))\left(2\|w\|_{\mathbf{L}^\infty(\mathbb{R}_-;\mathbb{R})} + \Delta x(j_c-j_w)\mathrm{Lip}(w)\right)\right.$. □

We are now in a position to prove a convergence result for the scheme (3.1)−(3.3).

Theorem 3.3. *Under the CFL condition (3.8) and if w belongs to $\mathbf{Lip}(\mathbb{R}_-;\mathbb{R}_+)$, the constrainted finite volume scheme (3.1)–(3.3) converges in $\mathbf{L}^1(Q)$ to the unique entropy solution to (1.1).*

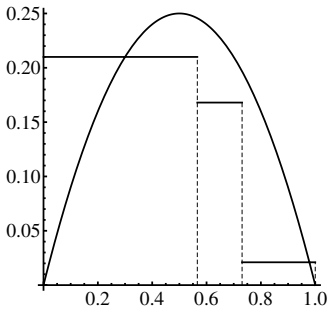

FIGURE 1. The functions $[\rho \mapsto f(\rho)]$ and $[\xi \mapsto p(\xi)]$ as in Section 3.3.

Proof. Let (ρ_Δ, q_Δ) be constructed by the scheme (3.1)–(3.3). Proposition 3.2 and Helly's lemma give the existence of a subsequence, still denoted q_Δ and a constraint function $q \in \mathbf{L}^\infty([0,T])$ such that q_Δ converges to q strongly in $\mathbf{L^1}([0,T])$ as $\Delta t \to 0$. Let $\rho \in \mathbf{L}^\infty(\mathbb{R}_+ \times \mathbb{R}; [0,R])$ be the unique entropy solution to (1.1a), (1.1b) and (2.1) associated to q. It remains to prove that the subsequence ρ_Δ converges to ρ strongly in $\mathbf{L^1}(Q)$ as Δt, $\Delta x \to 0$. The uniqueness of the entropy solution to (1.1a), (1.1b) and (2.1) will then imply that the full sequence ρ_Δ converges to ρ and, as a consequence, the full sequence q_Δ converges to $q = p\left(\int_{\mathbb{R}_-} w(x)\,\rho(t,x)\,\mathrm{d}x\right)$.

Let $\hat{q}_\Delta$ be a piecewise constant approximation of q such that $\hat{q}_\Delta$ converges to q strongly in $\mathbf{L^1}([0,T])$. Furthermore, we also introduce $\hat{\rho}_\Delta$ constructed by the scheme (3.1)–(3.2) and associated to $\hat{q}_\Delta$. Now we have

$$\|\rho - \rho_\Delta\|_{\mathbf{L^1}(Q)} \leq \|\rho - \hat{\rho}_\Delta\|_{\mathbf{L^1}(Q)} + \|\rho_\Delta - \hat{\rho}_\Delta\|_{\mathbf{L^1}(Q)}.$$

But, thanks to ([3], Thm. 4.9), under the CFL condition (3.8), $\|\rho - \hat{\rho}_\Delta\|_{\mathbf{L^1}(Q)}$ tends to 0 as Δt, $\Delta x \to 0$. Furthermore, thanks to Proposition 3.1, we have

$$\|\rho_\Delta - \hat{\rho}_\Delta\|_{\mathbf{L^1}(Q)} \leq 2\ T\ \|q_\Delta - \hat{q}_\Delta\|_{\mathbf{L^1}([0,T])}$$

which shows that also $\|\rho_\Delta - \hat{\rho}_\Delta\|_{\mathbf{L^1}(Q)}$ tends to 0 as Δt, $\Delta x \to 0$. □

3.3. Validation of the numerical scheme

We propose here to validate the numerical scheme (3.1)–(3.3) by using the Godounov numerical flux (see *e.g.* [19, 28]) which will be used in the remaining of this paper:

$$F(a,b) = \begin{cases} \min\limits_{[a,b]} f & \text{if } a \leq b, \\ \max\limits_{[b,a]} f & \text{if } a > b. \end{cases}$$

We consider the explicit solution to (1.1) constructed in ([5], Sect. 6) by applying the wave-front tracking algorithm. The set up for the simulation is as follows. Consider the domain of computation $[-6,1]$, take a normalized flux $f(\rho) = \rho(1-\rho)$ (namely the maximal velocity and the maximal density are assumed to be equal to one) and a linear weight function $w(x) = 2(1+x)\,\chi_{[-1,0]}(x)$. Assume a uniform distribution of maximal density in $[x_A, x_B] \subset]-6,0[$ at time $t = 0$, namely $\bar{\rho} = \chi_{[x_A,x_B]}$. The efficiency of the exit, p, see Figure 1, is of the form

$$p(\xi) = \begin{cases} p_0 & \text{if } 0 \leq \xi < \xi_1, \\ p_1 & \text{if } \xi_1 \leq \xi < \xi_2, \\ p_2 & \text{if } \xi_2 \leq \xi \leq 1. \end{cases}$$

The explicit solution ρ corresponding to the values

$$p_0 = 0.21, \qquad p_1 = 0.168, \qquad p_2 = 0.021, \qquad \xi_1 \sim 0.566,$$
$$x_A = -5.75, \qquad x_B = -2, \qquad \xi_2 \sim 0.731,$$

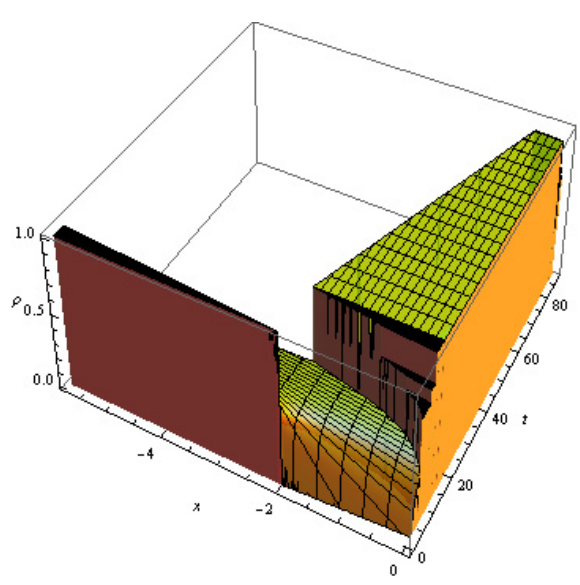

(a) The solution in the (t, x, ρ)-coordinates.

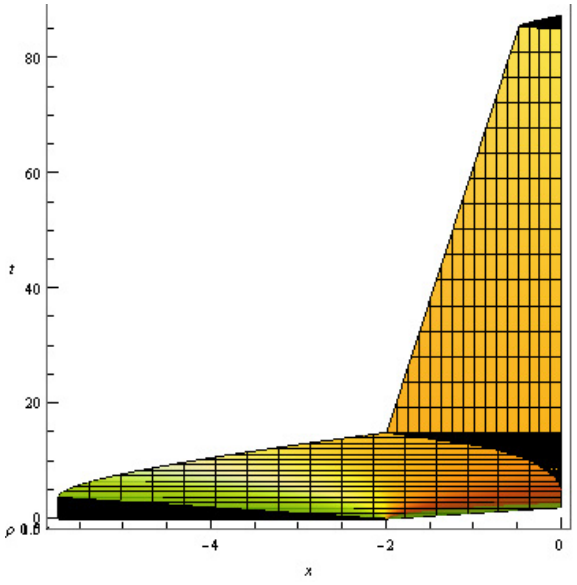

(b) The solution in the (x, t)-coordinates.

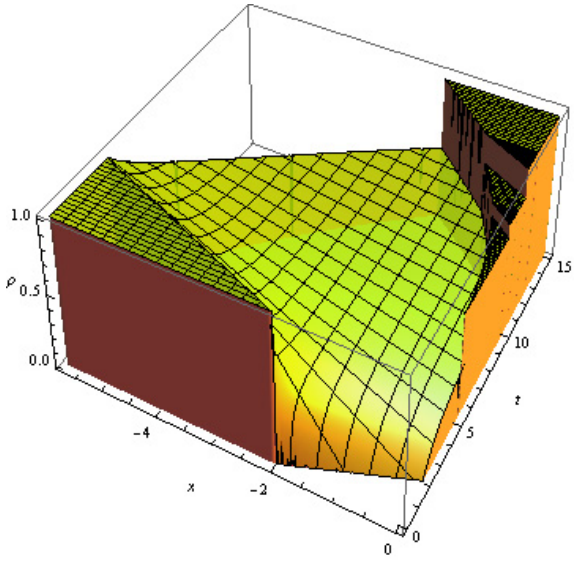

(c) The solution in the (t, x, ρ)-coordinates for $0 \leq t \leq 15$.

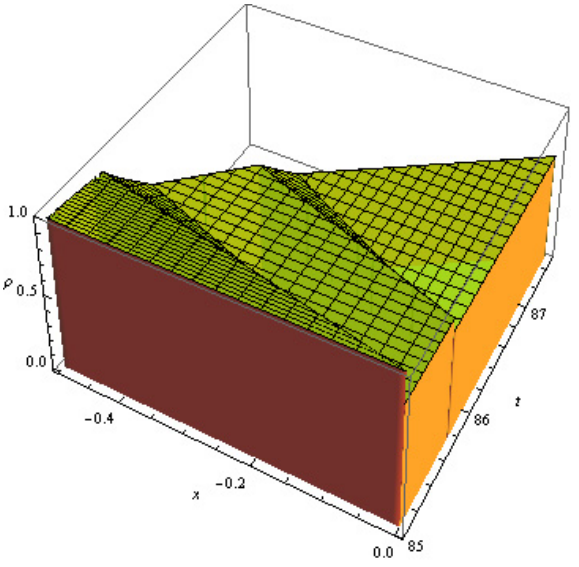

(d) The solution in the (t, x, ρ)-coordinates for $85 \leq t \leq 87.5$.

FIGURE 2. Representation of the solution constructed in ([5], Sect. 6) and described in Section 3.3.

is represented in Figure 2. The above choices for the flux f and the efficiency p ensure that the solution to each Riemann problem is unique, see [6]. We refer to ([5], Sect. 6) for the details about the construction of the solution ρ and its physical interpretation.

A qualitative comparison between the numerically computed solution $x \mapsto \rho_\Delta(t, x)$ and the explicitly computed solution $x \mapsto \rho(t, x)$ at different fixed times t is in Figure 3. We observe good agreements between $x \mapsto \rho(t, x)$ and $x \mapsto \rho_\Delta(t, x)$. The parameters for the numerically computed solution are $\Delta x = 3.5 \times 10^{-4}$ and $\Delta t = 0.4\Delta x = 1.4 \times 10^{-4}$.

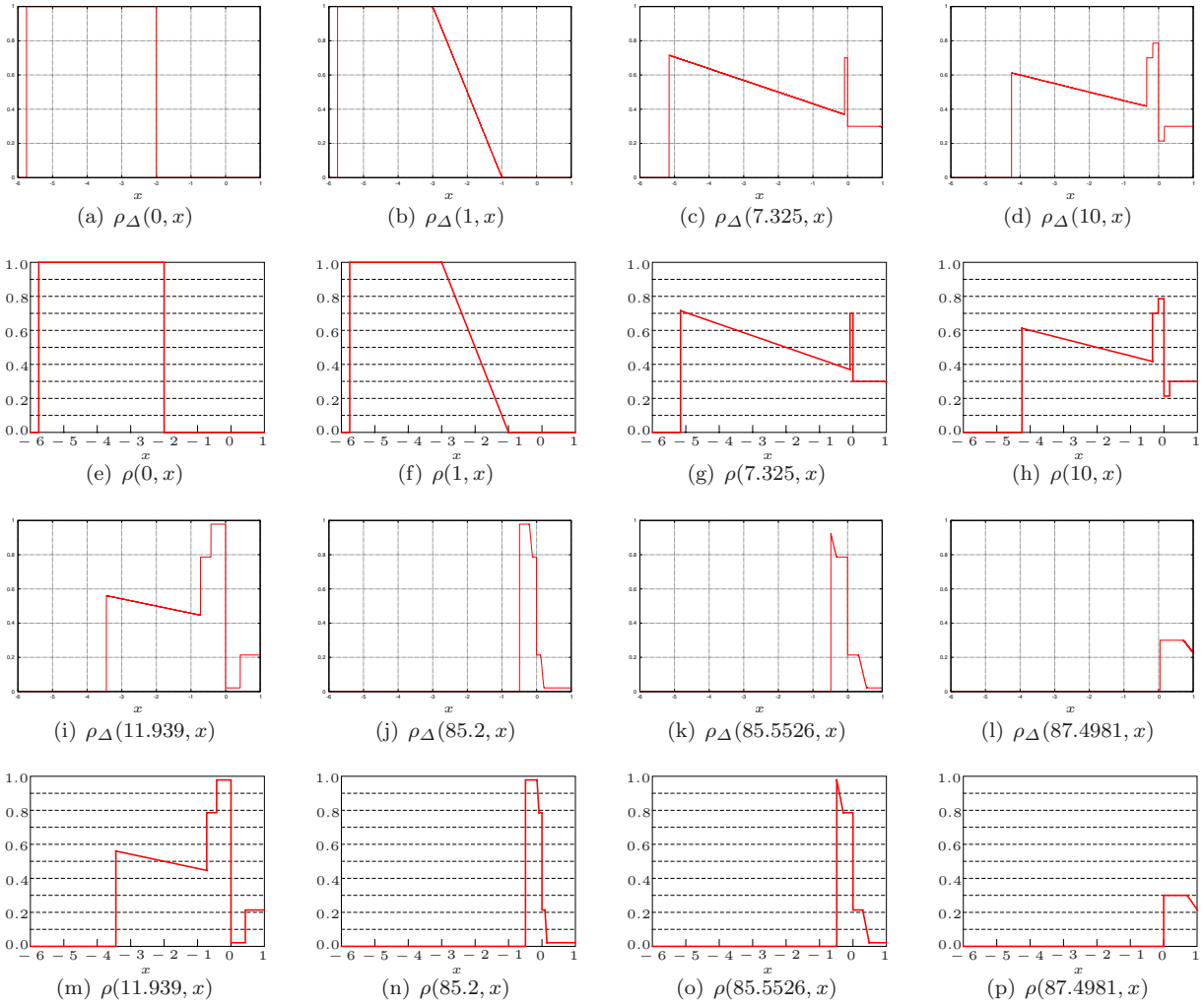

(a) $\rho_\Delta(0,x)$ (b) $\rho_\Delta(1,x)$ (c) $\rho_\Delta(7.325,x)$ (d) $\rho_\Delta(10,x)$

(e) $\rho(0,x)$ (f) $\rho(1,x)$ (g) $\rho(7.325,x)$ (h) $\rho(10,x)$

(i) $\rho_\Delta(11.939,x)$ (j) $\rho_\Delta(85.2,x)$ (k) $\rho_\Delta(85.5526,x)$ (l) $\rho_\Delta(87.4981,x)$

(m) $\rho(11.939,x)$ (n) $\rho(85.2,x)$ (o) $\rho(85.5526,x)$ (p) $\rho(87.4981,x)$

FIGURE 3. With reference to Section 3.3: The numerically computed solution $x \mapsto \rho_\Delta(t,x)$ and the explicitly computed solution $x \mapsto \rho(t,x)$ at different fixed times t.

A convergence analysis is also performed for this test. We introduce the relative $\mathbf{L^1}$-error for the density ρ, at a given time t^n, defined by

$$E^n_{\mathbf{L^1}} = \left[\sum_j \left|\rho(t^n,x_j) - \rho^n_j\right|\right] \Big/ \left[\sum_j \left|\rho(t^n,x_j)\right|\right].$$

In Table 1, we computed the relative $\mathbf{L^1}$-errors for different numbers of space cells at the fixed time $t = 10$. The time space is fixed to $\Delta t = 1.4 \times 10^{-4}$. We deduce that the order of convergence is approximatively 0.93. As in [3], we observe that the modification (3.2) of the numerical flux does not affect the accuracy of the scheme.

4. NUMERICAL SIMULATIONS

This section is devoted to the phenomenological description of some collective effects in crowd dynamics related to the capacity drop, namely the Faster Is Slower (FIS) effect and the Braess' paradox.

TABLE 1. Relative $\mathbf{L^1}$-error at time $t = 10$.

Number of cells	$\mathbf{L^1}$-error	Rate of convergence
625	1.1491×10^{-2}	–
1250	4.641×10^{-3}	1.3
2500	3.5968×10^{-3}	0.83
5000	1.5106×10^{-3}	0.91
10 000	8.1705×10^{-4}	0.92
20 000	4.243×10^{-4}	0.93

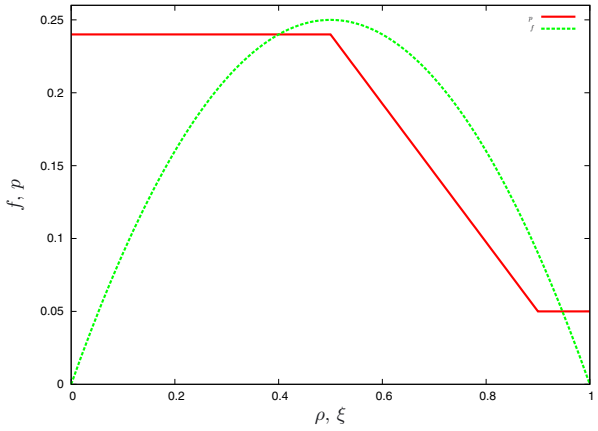

FIGURE 4. The normalized flux $\rho \to f(\rho)$ and the constraint $\xi \to p(\xi)$ defined in (4.1).

4.1. Faster is Slower effect

The FIS effect was first described in [21, 30] in the context of the room evacuation problem. The authors studied the evolution of the evacuation time as a function of the maximal velocity reached by the pedestrians, and they have shown that there exists an optimal velocity for which the evacuation time attains a minimum. Therefore, any acceleration beyond the optimal velocity worses the evacuation time. Following the studies above, the curve representing the evacuation time as a function of the average velocity takes a characteristic shape ([30], Fig. 1).

The first numerical tests we performed aim to verify if such shape is obtained starting from the ADR model. To this end, we consider the corridor modeled by the segment $[-6,1]$, with an exit at $x = 0$. We consider the flux $f(\rho) = \rho\, v_{\max}\,(1-\rho)$, where $v_{\max}$ is the maximal velocity of the pedestrians and the maximal density is equal to one. We use the same weight function as for the validation of the scheme, $w(x) = 2(1+x)\chi_{[-1,0]}(x)$ and, the same initial density, $\bar{\rho} = \chi_{[-5.75,-2]}$. The efficiency of the exit p is now given by the following continuous function

$$p(\xi) = \begin{cases} p_0 & \text{if } 0 \le \xi < \xi_1, \\ \dfrac{(p_0 - p_1)\xi + p_1\xi_1 - p_0\xi_2}{\xi_1 - \xi_2} & \text{if } \xi_1 \le \xi < \xi_2, \\ p_1 & \text{if } \xi_2 \le \xi \le 1, \end{cases} \tag{4.1}$$

where

$$p_0 = 0.24, \qquad p_1 = 0.05, \qquad \xi_1 = 0.5, \qquad \xi_2 = 0.9.$$

The space and time steps are fixed to $\Delta x = 5 \times 10^{-3}$ and $\Delta t = 5 \times 10^{-4}$. In Figure 4 are plotted the flux f corresponding to the maximal velocity $v_{\max} = 1$ and the above efficiency of the exit.

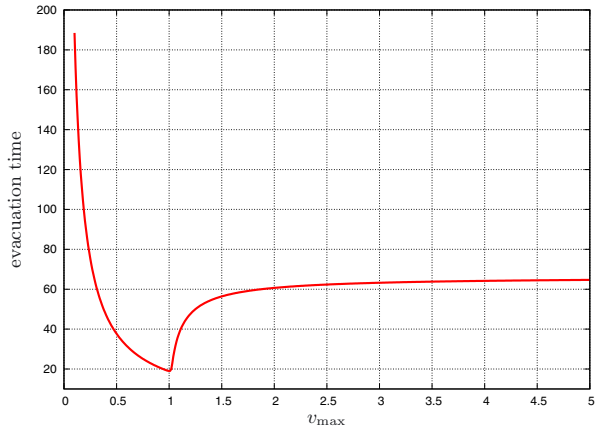

FIGURE 5. With reference to Section 4.1: Evacuation time as a function of the velocity $v_{\max}$.

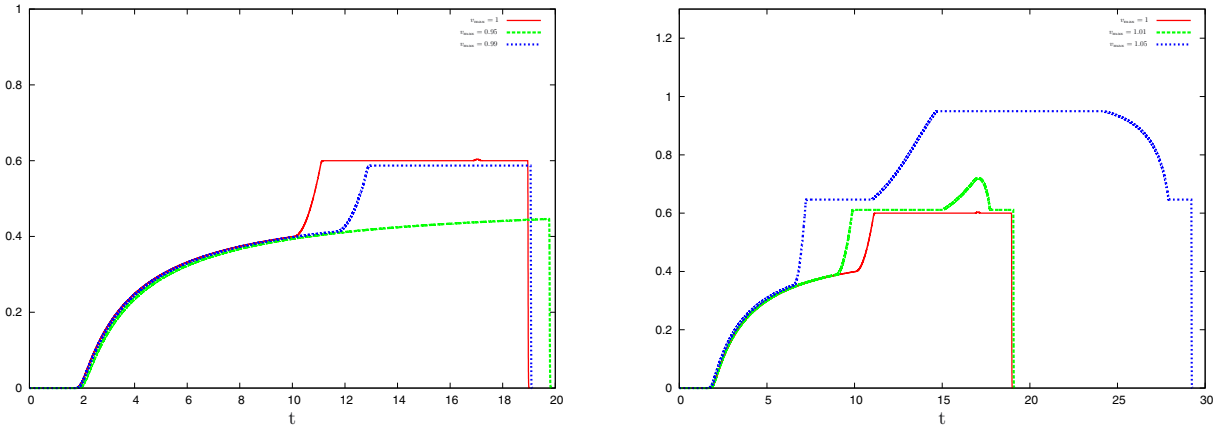

(a) $t \mapsto \rho_\Delta(0,t)$ for velocities $v_{\max} \leq 1$.

(b) $t \mapsto \rho_\Delta(0,t)$ for velocities $v_{\max} \geq 1$.

FIGURE 6. With reference to Section 4.1: Densities at the exit as a function of time for different velocities.

Figure 5 represents the evacuation time as a function of the maximal velocity $v_{\max}$, as $v_{\max}$ varies in the interval $[0.1, 5]$. As we can observe, the general shape described in ([30], Fig. 1) is recovered. The numerical minimal evacuation time is 19.007 and is obtained for $v_{\max} = 1$.

In addition, we present in Figure 6 the density at the exit as a function of time for different values of the maximal velocity $v_{\max}$ around the optimal one. We notice that the maximal density at the exit increases with the velocity. This expresses the jamming at the exit that leads to the FIS effect.

Then we performed some series of tests to see how the general shape obtained in Figure 5 changes with respect to variations of the parameters of the model. In Figure 8a, we show this variation when we consider different initial densities, namely, $\bar{\rho}$, $\bar{\rho}_1$ and $\bar{\rho}_2$ with $\bar{\rho}_1(x) = 0.8\chi_{[-5.75,-2]}$ and $\bar{\rho}_2(x) = 0.6\chi_{[-5.75,-2]}$. The general shape of the curves is conserved. We observe that the evacuation time increases with the initial amount of pedestrians while the optimal velocity decreases as the initial amount of pedestrians increases. The minimal evacuation time and the corresponding optimal maximal velocity are 12.259 and 1.07 for $\bar{\rho}_2$ and 15.691 and 1.03 for $\bar{\rho}_1$.

Next we explore the case where the efficiency of the exit varies. We consider the function p defined in (4.1) and the modification p_β such that $p_\beta(\xi) = p(\beta\xi)$. In Figure 7, we plotted the functions p, p_β for $\beta = 0.8$ and $\beta = 0.9$.

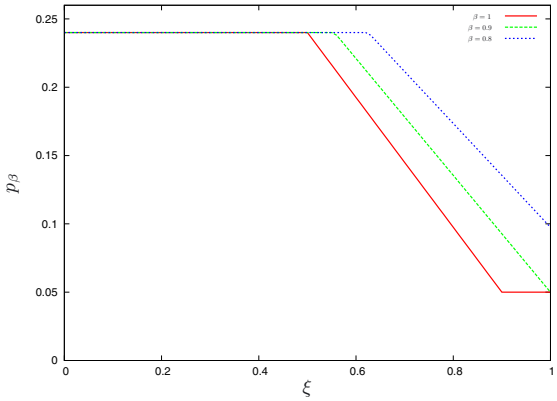

FIGURE 7. With reference to Section 4.1: The efficiencies $\xi \to p_\beta(\xi)$ for $\beta = 0.8, 0.9, 1$.

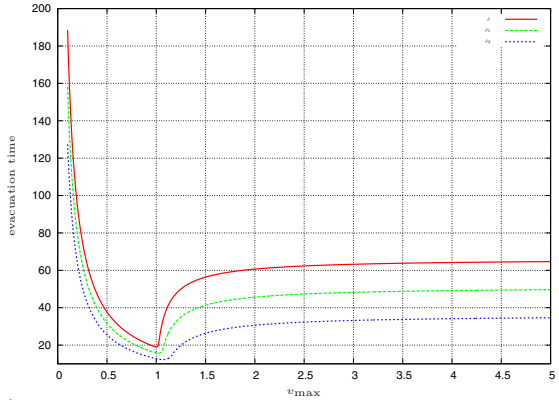

(a) Evacuation time as a function of $v_{\max}$ for different amounts of initial densities.

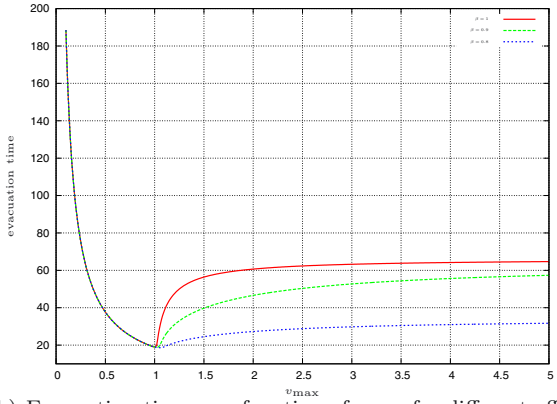

(b) Evacuation time as a function of $v_{\max}$ for different efficiencies of the exit.

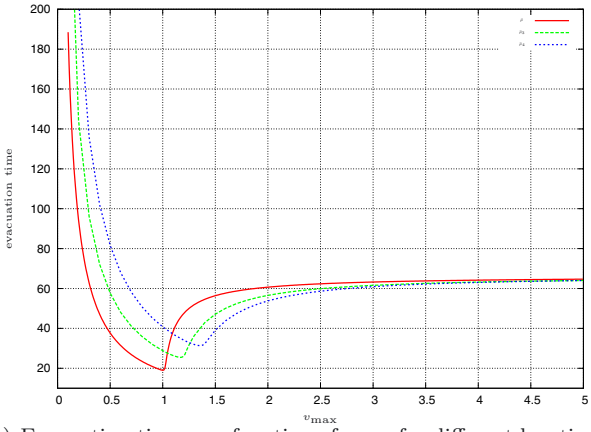

(c) Evacuation time as a function of $v_{\max}$ for different locations of the initial density.

FIGURE 8. With reference to Section 4.1: Evacuation time as a function of $v_{\max}$ for different parameters of the model.

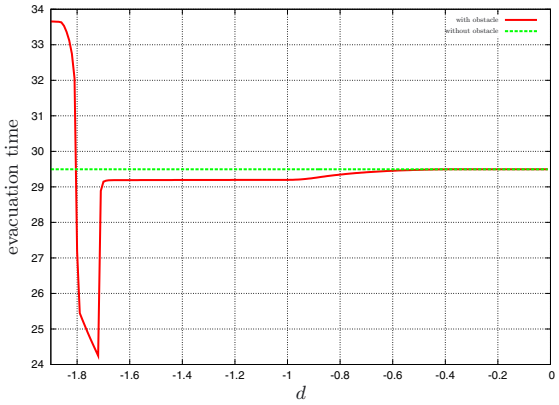

FIGURE 9. With reference to Section 4.2: Evacuation time as a function of the position of the obstacle.

Then, in Figure 8b are plotted the evacuation time curves corresponding to these three efficiencies of the exit. As minimum evacuation times, we obtain 18.586 and 18.827 for $\beta = 0.8, 0.9$ respectively. As expected, the minimal evacuation time increases with lower efficiency of the exit. The corresponding velocities are approximatively 1.06 and 1.02 respectively.

Finally, we change the location of the initial density. In addition to the corridor $[-6, 1]$, we consider two other corridors modeled by the segments $[-12, 1]$ and $[-20, 1]$. In these two corridors we take as initial densities $\bar{\rho}_3(x) = \chi_{[-11.75,-8]}$ and $\bar{\rho}_4(x) = \chi_{[-19.75,-16]}$ respectively. We have reported the obtained evacuation time curves in Figure 8c. As expected, the minimal evacuation time increases with the distance between the exit and the initial density location.

4.2. Braess' paradox

The presence of obstacles, such as columns upstream from the exit, may prevent the crowd density from reaching dangerous values and may actually help to minimize the evacuation time, since in a moderate density regime the full capacity of the exit can be exploited. From a microscopic point of view, the decrease of the evacuation time may seem unexpected, as some of the pedestrians are forced to choose a longer path to reach the exit.

The ADR model is able to reproduce the Braess' paradox for pedestrians, as we show in the following simulations. We consider, as in the previous subsection, the corridor modeled by the segment $[-6, 1]$ with an exit at $x = 0$. We compute the solution corresponding to the flux $f(\rho) = \rho(1 - \rho)$, the initial density $\bar{\rho}(x) = \chi_{[-5.75,-2]}(x)$, the efficiency of the exit p of the form (4.1) with the parameters

$$p_0 = 0.21, \qquad p_1 = 0.1, \qquad \xi_1 = 0.566, \qquad \xi_2 = 0.731$$

and the same weight function $w(x) = 2(1 + x)\chi_{[-1,0]}(x)$. The space and time steps are fixed to $\Delta x = 5 \times 10^{-3}$ and $\Delta t = 5 \times 10^{-4}$. Without any obstacle, the numerical evacuation time is 29.496. In these following simulations we place an obstacle at $x = d$, with $-2 < d < 0$. The obstacle reduces the capacity of the corridor and can be seen as a door, which we assume larger than the one at $x = 0$. Following these ideas we define an efficiency function $p_\kappa(\xi) = \kappa\, p(\xi)$, where $\kappa = 1.15$ and a weight function $w_d(x) = 2(x - d + 1)\chi_{[d-1,d]}(x)$ associated to the obstacle.

In Figure 9 we have reported the evolution of the evacuation time when the position of the obstacle varies in the interval $[-1.9, -0.01]$ with a step of 0.01. We get the characteristic shape already obtained in ([17], Fig. 13) for the model introduced in [13]. We observe that for $-1.8 \leq d \leq -1.72$, the evacuation time is much lower than in the absence of the obstacle. The optimal position of the obstacle is obtained for $d = -1.72$ and the corresponding evacuation time is 24.246. We compare in Figure 10 five snapshots of the solution without

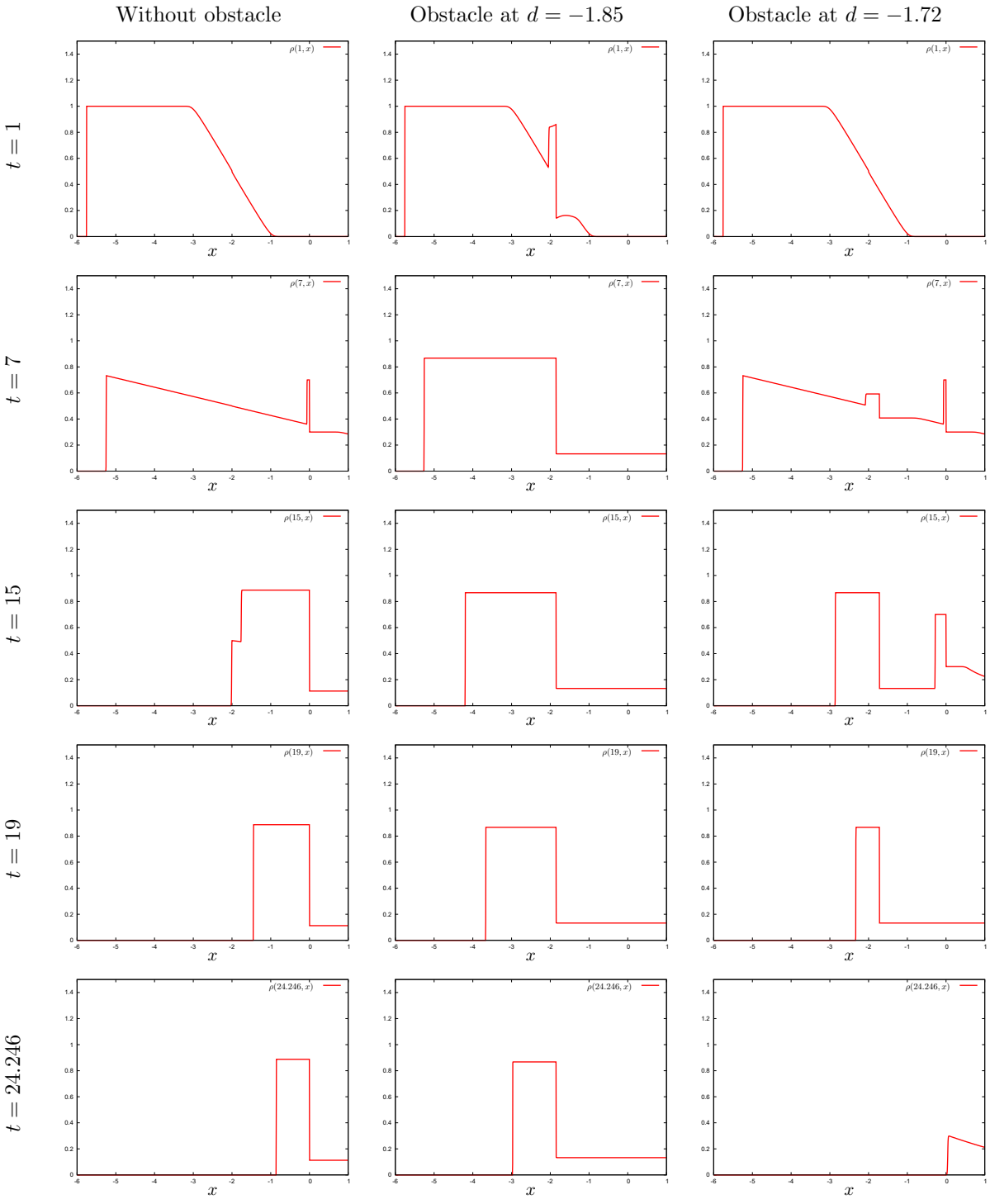

FIGURE 10. With reference to Section 4.2: Braess' paradox simulations: Density profiles at times $t = 1$ (*first line*), $t = 7$ (*second line*), $t = 15$ (*third line*), $t = 19$ (*fourth line*) and $t = 24.246$ (*last line*).

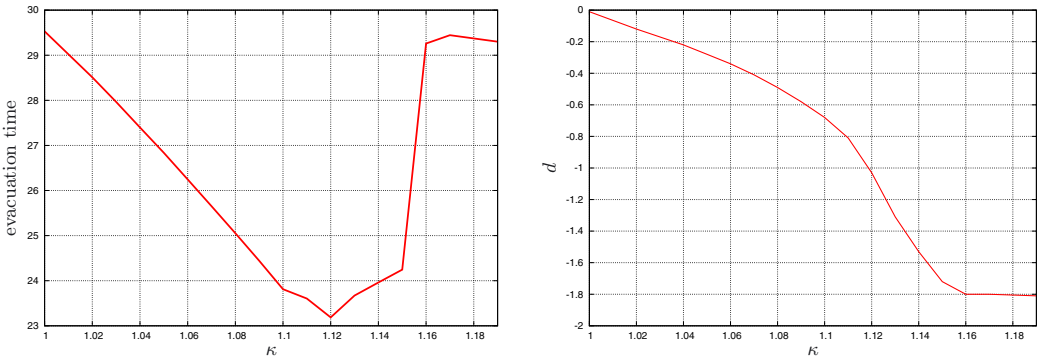

(a) Optimal evacuation time as a function of κ.

(b) Corresponding optimal distance d as a function of κ.

FIGURE 11. With reference to Section 4.2: Optimal evacuation time and corresponding optimal position of the obstacle as a function of the strength κ.

obstacle and the solutions with an obstacle placed at $d = -1.72$ and $d = -1.85$. This latter location corresponds to a case where the evacuation time is greater than the one without an obstacle. In these snapshots, we see that the obstacle placed at $d = -1.85$ becomes congested very soon. This is due to the fact that the obstacle is too close to the location of the initial density. When the obstacle is placed at $d = -1.72$, it mitigates the congestion at the exit.

So far we have fixed the coefficient κ to 1.15. In order to highlight the influence of κ, we performed simulations where we let now κ vary and for each value of κ, we used the position of the obstacle d as a parameter to minimize the associate evacuation time. Figure 11 shows the evolutions of the evacuation time and the corresponding optimal position of the obstacle when κ varies in $[1, 1.19]$. The interval is chosen so that the obstacle, interpreted as a door, is at least larger than the exit and has a capacity that is inferior to the one of the corridor. We observe the existence of an optimal value of κ, $\kappa = 1.12$ for which the evacuation time is $T = 23.187$ when the position of the obstacle is $d = -1.03$. From the extreme values of κ, we also see that, taking an obstacle with the same size as the exit or almost the same size as the corridor leads to optimal evacuation times that are close to the one without obstacle; we have $T = 29.53$ for $\kappa = 1$ and $T = 29.3$ for $\kappa = 1.19$. Finally we notice that the optimal distance between the obstacle and the exit is an increasing function of κ.

4.3. Zone of low velocity

In this section, we perform a series of simulations where the obstacle introduced in Section 4.2 is now replaced by a zone where the velocity of pedestrians is lower than elsewhere in the domain. The effect we want to observe here is similar to the one we see in Braess' paradox. Namely we prevent a high concentration of pedestrians in front of the exit by constraining their flow in an upstream portion of the corridor. In this case however the constraint is local, as the maximal value allowed for the flow only depends on the position in the corridor.

We consider again the corridor modeled by the segment $[-6, 1]$ with an exit at $x = 0$. The efficiency of the exit and the initial density are the same as in the previous subsection. Assume that the slow zone is of size one and is centred at $x = d$, where $-1.9 \leq d \leq 0$. Define the following function

$$k(x) = \begin{cases} 1 & \text{if } x \leq d - 0.5, \\ -2(x - d) & \text{if } d - 0.5 \leq x \leq d, \\ 2(x - d) & \text{if } d \leq x \leq d + 0.5, \\ 1 & \text{if } x \geq d + 0.5, \end{cases} \tag{4.2}$$

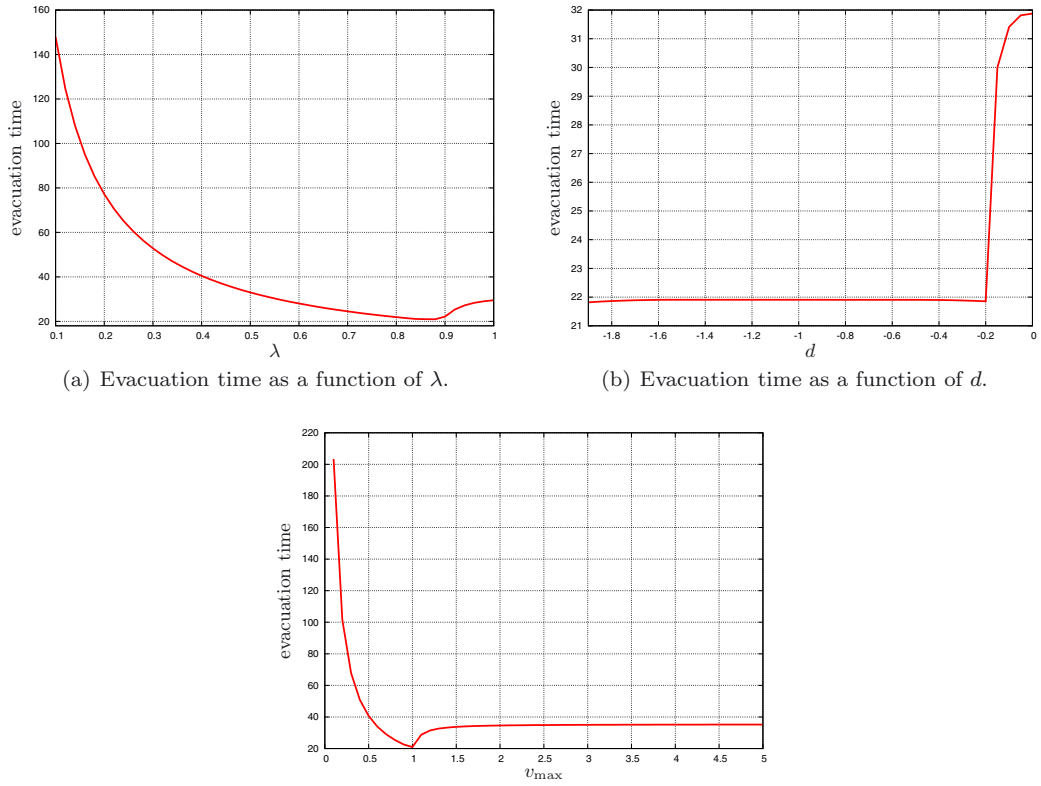

(a) Evacuation time as a function of λ.

(b) Evacuation time as a function of d.

(c) Evacuation time as a function of $v_{\max}$.

FIGURE 12. With reference to Section 4.3: Evacuation time as a function of different parameters of the model.

and the following velocity $v(x,\rho) = [\lambda + (1-\lambda)\,k(x)]\,v_{\max}\,(1-\rho)$, where $\lambda \in [0,1]$ and $v_{\max} \geq 1$ is the maximal velocity. With such velocity, the maximal velocity of pedestrians decreases in the interval $[d-0.5, d]$, reaching its minimal value $\lambda\, v_{\max}$ at $x = d$. Then the velocity increases in the interval $[d, d+0.5]$ reaching the maximum value $v_{\max}$, that corresponds to the maximal velocity away from the slow zone. Finally we consider the flux $f(x,\rho) = \rho\, v(x,\rho)$ and the space and time steps are fixed to $\Delta x = 5\times 10^{-3}$ and $\Delta t = 5\times 10^{-4}$. Let us underline that by definition f is Lipschitz.

Since the flux function considered here is Lipschitz continuous with respect to x, the x-dependence of the flux can be taken into account within the classical Kruzhkov theory which is easily combined with taking into account the constraint. From the numerical point of view, this generalization is also straightforward: we adapt the scheme presented in Section 3.1, by assuming a distinct flux function $f_{j+1/2}(\rho) = f(x_{j+1/2}, \rho)$ at each interface $x_{j+1/2}$ of the space grid. The reader can refer for instance to [8] and references therein for more details on finite volume methods with spatially varying flux functions.

Figure 12a shows the evolution of the evacuation time as a function of the parameter λ varying in the interval $[0.1, 1]$ when the center of the slow zone is fixed at $d = -1.5$. We observe that the optimal minimal velocity in the slow zone is for $\lambda = 0.88$ and the corresponding evacuation time is 20.945. Recalling that without the slow zone the evacuation time is 29.496, we see that the introduction of the slow zone allows to reduce the evacuation time. In Figure 12b, we show the evolution of the evacuation time when varying the center of the slow zone d in the interval $[-1.9, 0]$ and when the minimal and the maximal velocities are fixed and correspond to $\lambda = 0.88$

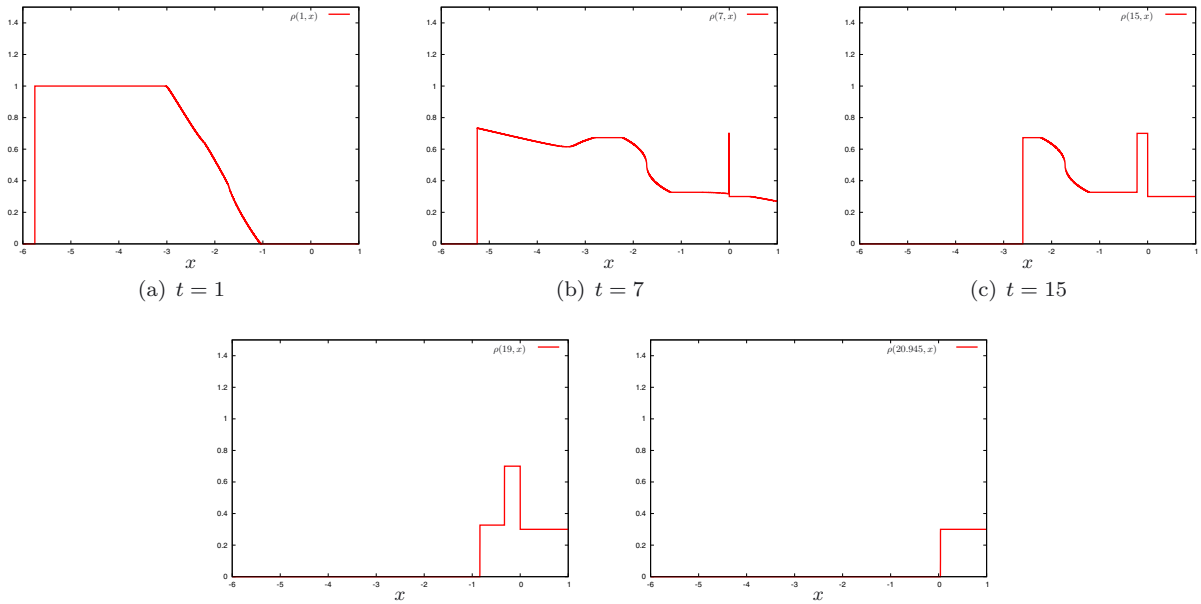

(a) $t = 1$ (b) $t = 7$ (c) $t = 15$

(d) $t = 19$ (e) $t = 20.945$

FIGURE 13. With reference to Section 4.3: Zone of low velocity simulations: density profiles at different times.

and $v_{\max} = 1$. We observe here that, unlike in the Braess' paradox test cases, the evacuation time does not depend on the location of the slow zone, except when this latter is close enough to the exit. Indeed, when the slow zone gets too close to the exit, the evacuation time grows. This is due to the fact that pedestrians do not have time to speed up before reaching the exit.

Fix now $d = -1.5$ and $\lambda = 0.88$ and assume that $v_{\max}$ varies in the interval $[0.1, 5]$. The evolution of the evacuation time as a function of $v_{\max}$ is reported in Figure 12c. We observe that we get the characteristic shape already obtained for the FIS effect in Section 4.1.

Finally we present in Figure 13 five snapshots of the solution computed with a zone of low velocity centered at $d = -1.72$, $\lambda = 0.88$ and $v_{\max} = 1$. In order to have a good resolution of this third solution, the space and time steps were fixed to $\Delta x = 3.5 \times 10^{-4}$ and $\Delta t = 7 \times 10^{-5}$. We note that in the case where a zone of low velocity is placed in the domain, the capacity drop at the exit is mitigated with respect to the cases with and without an obstacle, as the density of pedestrians never attains very high values in the region next to the exit. Moreover, the minimal evacuation time we obtain by introducing a zone of low velocity takes lower values than the ones obtained in Section 4.2, even when we take the optimal values of κ and of d. This is due to the fact that in all Braess' paradox simulations we can observe effects related to the capacity drop upstream the exit *and* upstream the obstacle. By construction, these phenomena cannot be observed upstream the zone of low velocity.

5. CONCLUSIONS

Qualitative features that are characteristic of pedestrians' macroscopic behaviour at bottlenecks (Faster is Slower, Braess' paradox) are reproduced in the setting of the simple scalar model with non-local point constraint introduced in [5]. These effects are shown to be persistent for large intervals of values of parameters. The validation is done by means of a simple and robust time-explicit splitting finite volume scheme which is proved to be convergent, with experimental rate close to one.

The results presented in this paper allow to consider more complex models. Indeed, as ADR is a first order model, it is not able to capture more complicated effects related to crowd dynamics. Typically, ADR fails to reproduce the amplification of small perturbations. This leads to consider second order model such as the model proposed by Aw *et al.* [7,37] in the framework of vehicular traffic.

Another extension of this work is to consider the ADR model with constraints that are non-local in time. Such constraints allow to tackle optimal management problems in the spirit of [16,18].

Finally, this work can also be extended to two-dimensional models where experimental validations may be possible.

Acknowledgements. All the authors are supported by French ANR JCJC grant CoToCoLa and Polonium 2014 (French-Polish cooperation program) No.331460NC. The second author is also supported by the Université de Franche-Comté, soutien aux EC 2014. The last author is also partially supported by Interdyscyplinarne Centrum Modelowania Matematycznego i Komputerowego, Uniwersytet Warszawski. The first author is grateful to IRMAR, Université de Rennes, for the hospitality during the preparation of this paper. The last author thanks Gran Sasso Science Institute, L'Aquila, and LMB Laboratoire de Mathématiques CNRS UMR6623, Université de Franche-Comté, for the hospitality during the preparation of this paper.

References

[1] B. Andreianov, New approches to describing admissibility of solutions of scalar conservation laws with discontinuous flux. *ESAIM Proc. Surv.* **50** (2015) 40–65.

[2] B. Andreianov and C. Cancès, On interface transmission conditions for conservation laws with discontinuous flux of general shape. *J. Hyperbolic Differ. Equ.* **12** (2015) 343–384.

[3] B. Andreianov, P. Goatin and N. Seguin, Finite volume schemes for locally constrained conservation laws. *Numer. Math.* **115** (2010) 609–645.

[4] B. Andreianov, K.H. Karlsen and N.H. Risebro, A theory of L^1-dissipative solvers for scalar conservation laws with discontinuous flux. *Arch. Ration. Mech. Anal.* **201** (2011) 27–86.

[5] B. Andreianov, C. Donadello and M.D. Rosini, Crowd dynamics and conservation laws with nonlocal constraints and capacity drop. *Math. Models Methods Appl. Sci.* **24** (2014) 2685–2722.

[6] B. Andreianov, C. Donadello, U. Razafison and M.D. Rosini, Riemann problems with non–local point constraints and capacity drop. *Math. Biosci. Eng.* **12** (2015) 259–278.

[7] A. Aw and M. Rascle, Resurrection of "second order" models of traffic flow. *SIAM J. Appl. Math.* **60** (2000) 916–938.

[8] D.S. Bale, R. Leveque, S. Mitran and J.A. Rossmanith, A wave propagation method for conservation laws and balance laws with spatially varying flux functions. *SIAM J. Sci. Comput.* **24** (2002) 955–978.

[9] E.M. Cepolina, Phased evacuation: An optimisation model which takes into account the capacity drop phenomenon in pedestrian flows. *Fire Safety J.* **44** (2009) 532–544.

[10] C. Cancès and N. Seguin, Error estimate for Godounov approximation of locally constrained conservation laws *SIAM J. Numer. Anal.* **50** (2012) 3036–3060.

[11] C. Chalons, Numerical Approximation of a Macroscopic Model of Pedestrian Flows. *SIAM J. Sci. Comput.* **29** (2007) 539–555.

[12] C. Chalons, P. Goatin and N. Seguin, General constrained conservation laws. Application to pedestrian flow modeling. *Netw. Heterog. Media* **8** (2013) 433–463.

[13] R.M. Colombo and M.D. Rosini, Pedestrian flows and non-classical shocks. *Math. Methods Appl. Sci.* **28** (2005) 1553–1567.

[14] R.M. Colombo and P. Goatin, A well posed conservation law with a variable unilateral constraint. *J. Differ. Equ.* **234** (2007) 654–675.

[15] R.M. Colombo and M.D. Rosini, Existence of nonclassical solutions in a Pedestrian flow model. *Nonlin. Anal. Real World Appl.* **10** (2009) 2716–2728.

[16] R.M. Colombo, G. Facchi, G. Maternini and M.D. Rosini, On the continuum modeling of crowds. In vol. 67 of *Hyperbolic Problems: Theory, Numerics and Applications, Proc. of Sympos. Appl. Math.* AMS, Providence, RI (2009) 517–526.

[17] R.M. Colombo, P. Goatin, and M.D. Rosini, A macroscopic model for pedestrian flows in panic situations. *GAKUTO Int. Series Math. Sci. Appl.* **32** (2010) 255–272.

[18] R.M. Colombo, P. Goatin and M.D. Rosini, On the modelling and management of traffic. *ESAIM: M2AN* **45** (2011) 853–872.

[19] E. Godlewski and P.-A. Raviart, Numerical approximation of hyperbolic systems of conservation laws. Springer Verlag, New York (1996).

[20] B.D. Greenshields, A Study of Traffic Capacity, In vol. 14 of *Proc. Highway Res. Board* (1934) 448–477.

[21] D. Helbing, I. Farkas and T. Vicsek, Simulating dynamical features of escape panic. *Nature* **407** (2000) 487–490.

[22] D. Helbing, A. Johansson and H.Z. Al-Abideen, Dynamics of crowd disasters: An empirical study. *Phys. Rev. E* **75** (2007) 046109.

[23] S.P. Hoogendoorn and W. Daamen, Pedestrian behavior at bottlenecks. *Transport. Sci.* **39** (2005) 147–159.
[24] R.L. Hughes, The flow of human crowds. *Annu. Rev. Fluid Mech.* **35** (2003) 169–182.
[25] V.A. Kopylow, *The study of people' motion parameters under forced egress situations*. Ph.D. thesis, Moscow Civil Engineering Institute (1974).
[26] T. Kretz, A. Grünebohm, M. Kaufman, F. Mazur and M. Schreckenberg, Experimental study of pedestrian counterflow in a corridor. *J. Statist. Mech.* **2006** (2006) P10001.
[27] S.N. Kruzhkov, First order quasilinear equations with several independent variables. *Mat. Sb.* **81** (1970) 228–255.
[28] R.J. LeVeque, Finite volume methods for hyperbolic problems. *Cambridge Texts in Applied Mathematics*. Cambridge University Press, Cambridge (2002).
[29] M.J. Lighthill and G.B. Whitham, On Kinematic Waves. II. A Theory of Traffic Flow on Long Crowded Roads. *Proc. Roy. Soc. London Ser. A* **229** (1995) 317–345.
[30] D.R. Parisi and C.O. Dorso, Microscopic dynamics of pedestrian evacuation. *Physica A* **354** (2005) 606–618.
[31] P.I. Richards, Shock waves on the highway. *Oper. Res.* **4** (1956) 42–51.
[32] M.D. Rosini, Nonclassical interactions portrait in a macroscopic pedestrian flow model. *J. Differ. Eq.* **246** (2009) 408–427.
[33] M.D. Rosini, *Macroscopic Models for Vehicular Flows and Crowd Dynamics: Theory and Applications*. Springer, Heidelberg (2013).
[34] A. Schadschneider, W. Klingsch, H. Klüpfel and T. Kretz, C. Rogsch and A. Seyfried, Evacuation Dynamics: Empirical Results, Modeling and Applications. In *Extreme Environmental Events*, edited by R.A. Meyers. Springer (2011) 517–550.
[35] A. Seyfried, T. Rupprecht, A. Winkens, O. Passon, B. Steffen, W. Klingsch and M. Boltes, Capacity Estimation for Emergency Exits and Bottlenecks. In *Interflam 2007* (2007) 247–258.
[36] S.A. Soria, R. Josens and D.R. Parisi, Experimental evidence of the "Faster is Slower" effect in the evacuation of ants. *Safety Sci.* **50** (2012) 1584–1588.
[37] H.M. Zhang, A non-equilibrium traffic model devoid of gas-like behavior. *Transport. Res. Part B* **36** (2002) 275–290.
[38] X.L. Zhang, W.G. Weng, H.Y. Yuan and J.G. Chen, Empirical study of a unidirectional dense crowd during a real mass event. *Physica. A* **392** (2013) 2781–2791.